International Journal of Heat and Mass Transfer 52 (2009) 2215–2223

Contents lists available at ScienceDirect

International Journal of Heat and Mass Transfer

journal homepage: www.elsevier.com/locate/ijhmt

Conjugate natural convection with radiation in an enclosure

G.V. Kuznetsov [a], M.A. Sheremet [b,*]

[a] Faculty of Thermal Power Engineering, Tomsk Polytechnic University, 30, Lenin Avenue, 634050 Tomsk, Russia
[b] Faculty of Mechanics and Mathematics, Tomsk State University, 36, Lenin Avenue, 634050 Tomsk, Russia

ARTICLE INFO

Article history:
Received 21 November 2008
Available online 3 February 2009

Keywords:
Conjugate heat transfer
Natural convection
Radiation
Rosseland approximation
Heat source
Enclosure

ABSTRACT

Convective-radiative heat transfer in an enclosure having finite thickness heat-conducting walls at local heating at the bottom of the cavity has been numerically studied. Heat exchange with an environment due to convection and radiation has been considered on one of external sides of the decision region. The effect of parameters such as the Grashof number, the transient factor, the optical thickness and the solid wall thermal conductivity both on the local thermo-hydrodynamic characteristics such as streamlines and temperature fields and on the integral parameter like the average Nusselt number on the heat source surface has been analysed.

1. Introduction

There are many researches devoted to natural convection in enclosures [1–6]. The typical thermo-hydrodynamic modes describing formation and evolution of vortex structures and also dynamics of temperature fields were evolved. The theoretical substantiation of many experimental results was made. But practically the investigations of interference of natural convection in a fluid and heat conduction in a solid have a success [7,8]. The conjugate heat transfer problems concern both to building thermal physics [9] and to microelectronics [10,11]. There are few solutions of such problems [11–15]. The effects of wall heat conduction on natural convection in a two-dimensional square cavity having finite wall conductances in which air was used as the working fluid were experimentally and numerically investigated [12]. The results were obtained for a case of two isothermal and two adiabatic walls without taking possible convective heat exchange with an environment into account. Natural convection in open cavities with a discrete heater located on a vertical wall of finite thickness was numerically studied [11]. The optimum position of a discrete heater was ascertained to depend on the Rayleigh number, the thermal conductivity ratio of the wall, the aspect ratio of the cavity and the wall thickness. The essential effect of walls thickness on thermo-hydrodynamic parameters both in a square enclosure [13] and in a semicircular cavity [14] was revealed. Experimental measurements and numerical simulations of turbulent Rayleigh–Bénard convection of water in a cubical cavity having finite thickness walls were studied in [15]. Typical velocity and temperature fields describing the effects of the Rayleigh number and of the walls heat conductivity were obtained.

The objective of the present study is mathematical simulation of natural convection and radiation in the gas cavity and heat conduction in the walls of an enclosure at the presence of heat source on the bottom of the cavity and on the assumption of convective-radiative heat exchange with an environment.

2. Statement of the problem and method of solution

The schematic view of the geometry considered in the present study is given in Fig. 1.

It is an enclosure bounded by solid walls with a finite thickness and conductivity. The heat source located on the bottom of the cavity is kept at constant temperature. The convective-radiative heat exchange with an environment is modeled on one of the external sides ($x = 0$). Other external sides are assumed to be adiabatic.

It is supposed in the analysis that the thermophysical properties of the solid walls and of the fluid are independent of temperature, and the flow is laminar. The fluid is Newtonian, viscous, heat-conducting, radiating, and the Boussinesq approximation is valid. The fluid motion and heat transfer in the cavity are assumed to be three-dimensional. Radiation heat exchange by heat source and between the walls is modeled on basis of the optically thick layer approximation (Rosseland approximation) [16]. In Rosseland approach [16] the emitting medium can be considered like some continuum of photons, i.e. it is possible to assume, that on any element of medium, as well as in case of molecular conduction, only its neighboring elements directly influence. In such

* Corresponding author. Tel.: +7 3822 412 462; fax: +7 3822 529 740.
E-mail address: Michael-sher@yandex.ru (M.A. Sheremet).

0017-9310/$ - see front matter © 2008 Elsevier Ltd. All rights reserved.
doi:10.1016/j.ijheatmasstransfer.2008.12.006

Nomenclature

$Bi_1 = hL_x/k_1$ Biot number for the solid wall
$Fo_1 = \alpha_1 t_0/L_x^2$ Fourier number for the solid wall
g_x acceleration of gravity (x-projection)
g_y acceleration of gravity (y-projection)
g_z acceleration of gravity (z-projection)
$Gr = g_z\beta(T_{hs} - T_0)L_x^3/\nu^2$ Grashof number
h heat transfer coefficient
k_1 thermal conductivity of the solid wall
k_2 thermal conductivity of the gas
$k_{2,1} = k_2/k_1$ thermal conductivity ratio
L_x length of the gas cavity along x-axis
$N = \varepsilon\sigma L(T_{hs}\text{-}T_0)^3/k$ Stark number for the gas cavity
$N_1 = \varepsilon_1\sigma L_x(T_{hs}\text{-}T_0)^3/k_1$ Stark number for the solid wall
$Pr = \nu/\alpha$ Prandtl number
t time
t_0 time scale
T_0 initial temperature
T^e environmental temperature
T_{hs} heat source temperature
u, v, w velocity components in x, y, z directions
U, V, W dimensionless velocity components in X, Y, Z directions
V_0 velocity scale (convection velocity)
x, y, z Cartesian coordinates
X, Y, Z dimensionless Cartesian coordinates

Greek symbols
α thermal diffusivity
β coefficient of volumetric thermal expansion
ε specific emissitivity factor for the gas cavity
ε_1 specific emissitivity factor at solid wall surface $X = 0$
$\zeta = T_0/(T_{hs}\text{-}T_0)$ temperature parameter
Θ dimensionless temperature
κ_λ absorption coefficient
ν kinematic viscosity
σ Stephen-Boltzman constant
τ dimensionless time
τ_λ monochromatic optical thickness
ψ_x,ψ_y,ψ_z components of vector potential
ψ_0 vector potential scale
Ψ_x,Ψ_y,Ψ_z dimensionless components of vector potential
$\omega_x,\omega_y,\omega_z$ components of vorticity vector
ω_0 vorticity vector scale
$\Omega_x,\Omega_y,\Omega_z$ dimensionless components of vorticity vector

Subscripts
i number of the Cartesian basis vector
e environment
hs heat source

conditions, radiant energy transfer in medium can be likened to diffusion transfer.

Heat transfer process in the considered area (Fig. 1) is governed by the system of unsteady three-dimensional convection equations in the Boussinesq approximation in the gas cavity [2,4,5], where an item in the energy equation describing radiation is determined on the basis of Rosseland approximation [16]. The unsteady three-dimensional energy equation [17] with nonlinear boundary conditions is used for simulation of heat conduction in the solid walls.

The mathematical model is formulated in the dimensionless variables such as vector potential functions, vorticity vector and temperature [18–20].

The length of the gas cavity along x-axis is chosen as the scale distance. For the reduction to the dimensionless form of the equations system following correlations are used:

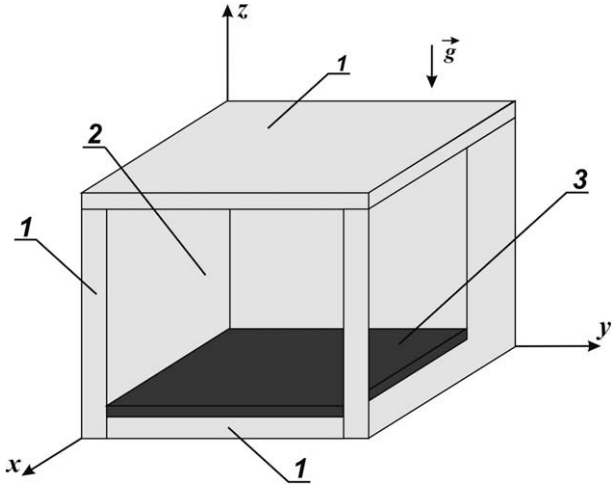

Fig. 1. Schematic view of the problem: *1* – walls; *2* – gas; *3* – heat source.

$$X = x/L_x, Y = y/L_x, Z = z/L_x, \tau = t/t_0, U = u/V_0, V = v/V_0, W = w/V_0,$$
$$\Theta = (T - T_0)/(T_{hs} - T_0), \Psi_x = \psi_x/\psi_0, \Psi_y = \psi_y/\psi_0, \Psi_z = \psi_z/\psi_0, \Omega_x = \omega_x/\omega_0,$$
$$\Omega_y = \omega_y/\omega_0, \Omega_z = \omega_z/\omega_0, \omega_0 = V_0/L_x, \psi_0 = V_0 L_x, V_0 = \sqrt{g_z\beta(T_{hs} - T_0)L_x};$$

Based on the above-mentioned assumptions, the non-dimensional form of the governing equations for the fluid can be written as follows:

$$\frac{\partial\Omega_x}{\partial\tau} + U\frac{\partial\Omega_x}{\partial X} + V\frac{\partial\Omega_x}{\partial Y} + W\frac{\partial\Omega_x}{\partial Z} - \Omega_x\frac{\partial U}{\partial X} - \Omega_y\frac{\partial U}{\partial Y} - \Omega_z\frac{\partial U}{\partial Z} = \frac{1}{\sqrt{Gr}}\nabla^2\Omega_x + \frac{\partial\Theta}{\partial Y} \quad (1)$$

$$\frac{\partial\Omega_y}{\partial\tau} + U\frac{\partial\Omega_y}{\partial X} + V\frac{\partial\Omega_y}{\partial Y} + W\frac{\partial\Omega_y}{\partial Z} - \Omega_x\frac{\partial V}{\partial X} - \Omega_y\frac{\partial V}{\partial Y} - \Omega_z\frac{\partial V}{\partial Z} = \frac{1}{\sqrt{Gr}}\nabla^2\Omega_y - \frac{\partial\Theta}{\partial X} \quad (2)$$

$$\frac{\partial\Omega_z}{\partial\tau} + U\frac{\partial\Omega_z}{\partial X} + V\frac{\partial\Omega_z}{\partial Y} + W\frac{\partial\Omega_z}{\partial Z} - \Omega_x\frac{\partial W}{\partial X} - \Omega_y\frac{\partial W}{\partial Y} - \Omega_z\frac{\partial W}{\partial Z} = \frac{1}{\sqrt{Gr}}\nabla^2\Omega_z \quad (3)$$

$$\nabla^2\Psi_x = -\Omega_x \quad (4)$$

$$\nabla^2\Psi_y = -\Omega_y \quad (5)$$

$$\nabla^2\Psi_z = -\Omega_z \quad (6)$$

$$\frac{\partial\Theta}{\partial\tau} + U\frac{\partial\Theta}{\partial X} + V\frac{\partial\Theta}{\partial Y} + W\frac{\partial\Theta}{\partial Z} = \frac{1}{\mathrm{Pr}\sqrt{Gr}}\nabla^2\Theta + \frac{16N}{3\tau_\lambda\mathrm{Pr}\sqrt{Gr}} \times \left\{3(\Theta+\zeta)^2\left[\left(\frac{\partial\Theta}{\partial X}\right)^2 + \left(\frac{\partial\Theta}{\partial Y}\right)^2 + \left(\frac{\partial\Theta}{\partial Z}\right)^2\right] + (\Theta+\zeta)^3\nabla^2\Theta\right\} \quad (7)$$

Energy equation for the solid walls

$$\frac{\partial\Theta_1}{\partial Fo_1} = \nabla^2\Theta_1 \quad (8)$$

Equations (1)–(8) are subjected to the following initial and boundary conditions.

Initial conditions are

$$\Psi_x(X,Y,Z,0)=0,\Psi_y(X,Y,Z,0)=0,\Psi_z(X,Y,Z,0)=0,$$
$$\Omega_x(X,Y,Z,0)=0,\Omega_y(X,Y,Z,0)=0,\Omega_z(X,Y,Z,0)=0,$$

$\Theta(X,Y,Z,0)=0$ except temperature for heat source on which $\Theta=1$ during the whole process time.

Boundary conditions are:

- convective-radiative heat exchange with an environment is modeled at the wall $X=0$

$$\frac{\partial\Theta_1(X,Y,Z,\tau)}{\partial X}=Bi_1\cdot\Theta_1(X,Y,Z,\tau)+Bi_1\cdot\frac{T_0-T^e}{T_{hs}-T_0}+Q_1,$$
$$Q_1=N_1\cdot\left[(\Theta_1(X,Y,Z,\tau)+\zeta)^4-\left(\frac{T^e}{T_{hs}-T_0}\right)^4\right],X=0;$$

- at the rest external walls for the equation (8) heat insulation conditions are set

$$\frac{\partial\Theta_1(X,Y,Z,\tau)}{\partial X^i}=0,\quad X^1\equiv X,X^2\equiv Y,X^3\equiv Z;$$

- at the solid–fluid interfaces parallel to plane XZ:

$$\Psi_x=\frac{\partial\Psi_y}{\partial Y}=\Psi_z=0,\begin{cases}\Theta_1=\Theta_2,\\ \frac{\partial\Theta_1}{\partial Y}=k_{2,1}\frac{\partial\Theta_2}{\partial Y};\end{cases}$$

- at the solid–fluid interfaces parallel to planeXY:

$$\Psi_x=\Psi_y=\frac{\partial\Psi_z}{\partial Z}=0,\begin{cases}\Theta_1=\Theta_2,\\ \frac{\partial\Theta_1}{\partial Z}=k_{2,1}\frac{\partial\Theta_2}{\partial Z};\end{cases}$$

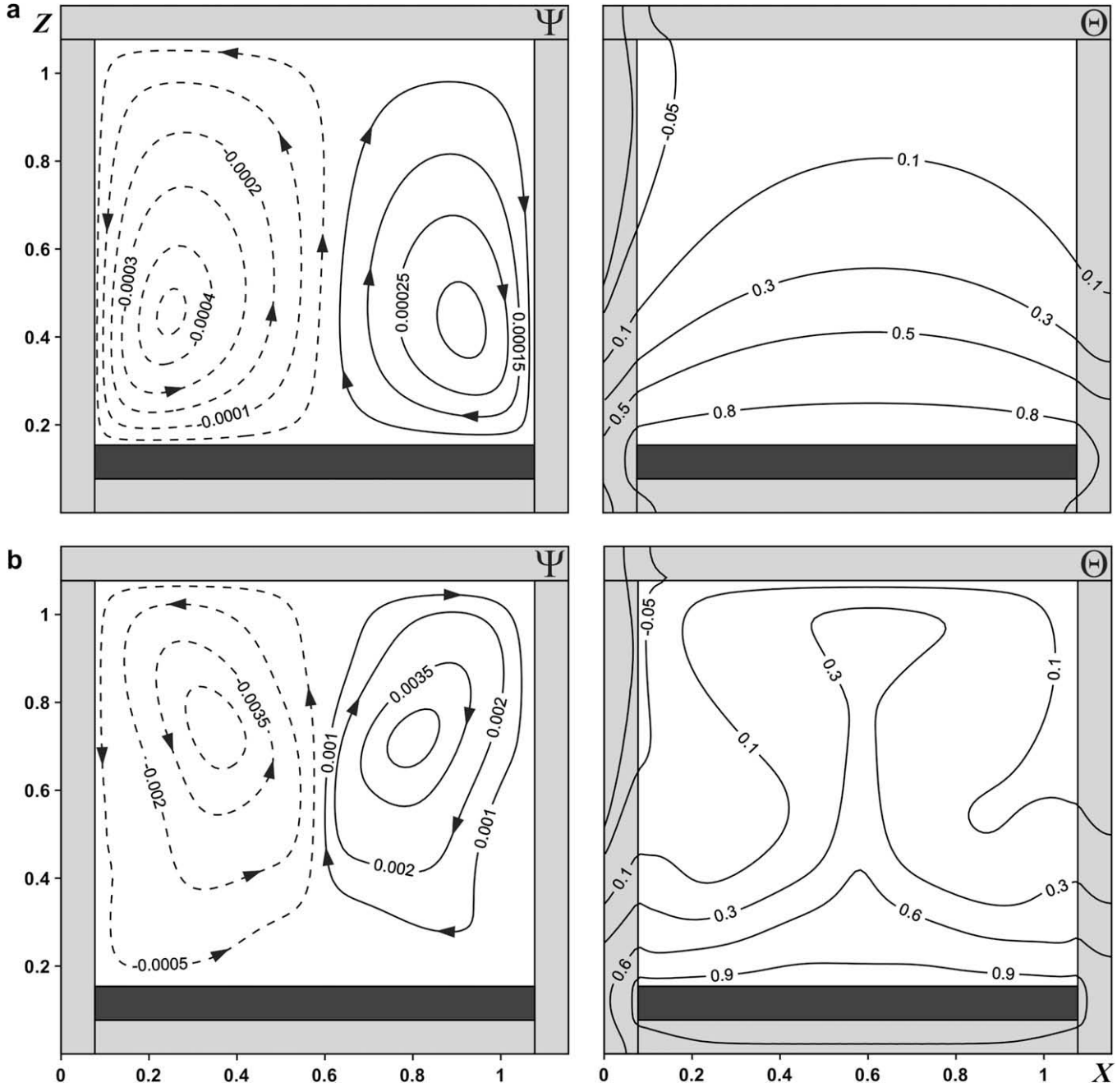

Fig. 2. Streamlines Ψ and isotherms Θ at $Y=0.3$, $\tau=300$, $\tau_\lambda=50$, $k_{2,1}=0.037$: $Gr=10^5$ – *a*, $Gr=10^7$ – *b*.

• at the solid–fluid interfaces parallel to plane *YZ*:

$$\frac{\partial \Psi_x}{\partial X} = \Psi_y = \Psi_z = 0, \begin{cases} \Theta_1 = \Theta_2, \\ \frac{\partial \Theta_1}{\partial X} = k_{2,1} \frac{\partial \Theta_2}{\partial X}. \end{cases}$$

Equations (1)–(8) with corresponding initial and boundary conditions has been solved by means of finite differences method [20–22].

The method of solution was tested for different cases, natural convection [23–25] and conjugate [26] problems. The results were in good agreement [22] with published data.

3. Results and discussion

Numerical analysis of the boundary value problem (1)–(8) has been carried out at following dimensionless complexes such as $Gr = 10^5$–10^7, Pr = 0.7, τ_λ = 50, 100, ∞, $k_{2,1}$ = , 0.037, 0.0037, describing the basic modes of convective-radiative heat transfer in enclosures. Dimensionless defining temperatures were $\Theta^e = -1$, $\Theta_{hs} = 1$, $\Theta_0 = 0$.

3.1. Effect of the Grashof number

Streamlines and temperature fields at different values of the Grashof number at $\tau = 300$, $Y = 0.3$ are presented in Fig. 2. The direction of gas motion in the gas cavity is indicated by arrows on streamlines.

Two convective cells are formed in the gas cavity at $Y = 0.3$ for $Gr = 10^5$ (Fig. 2, *a*). The reason for the appearance of these cells is both the heat source located on the bottom of the gas cavity and convective-radiative heat exchange at external boundary $X = 0$. The whirl representing the counter-clockwise gas motion, different

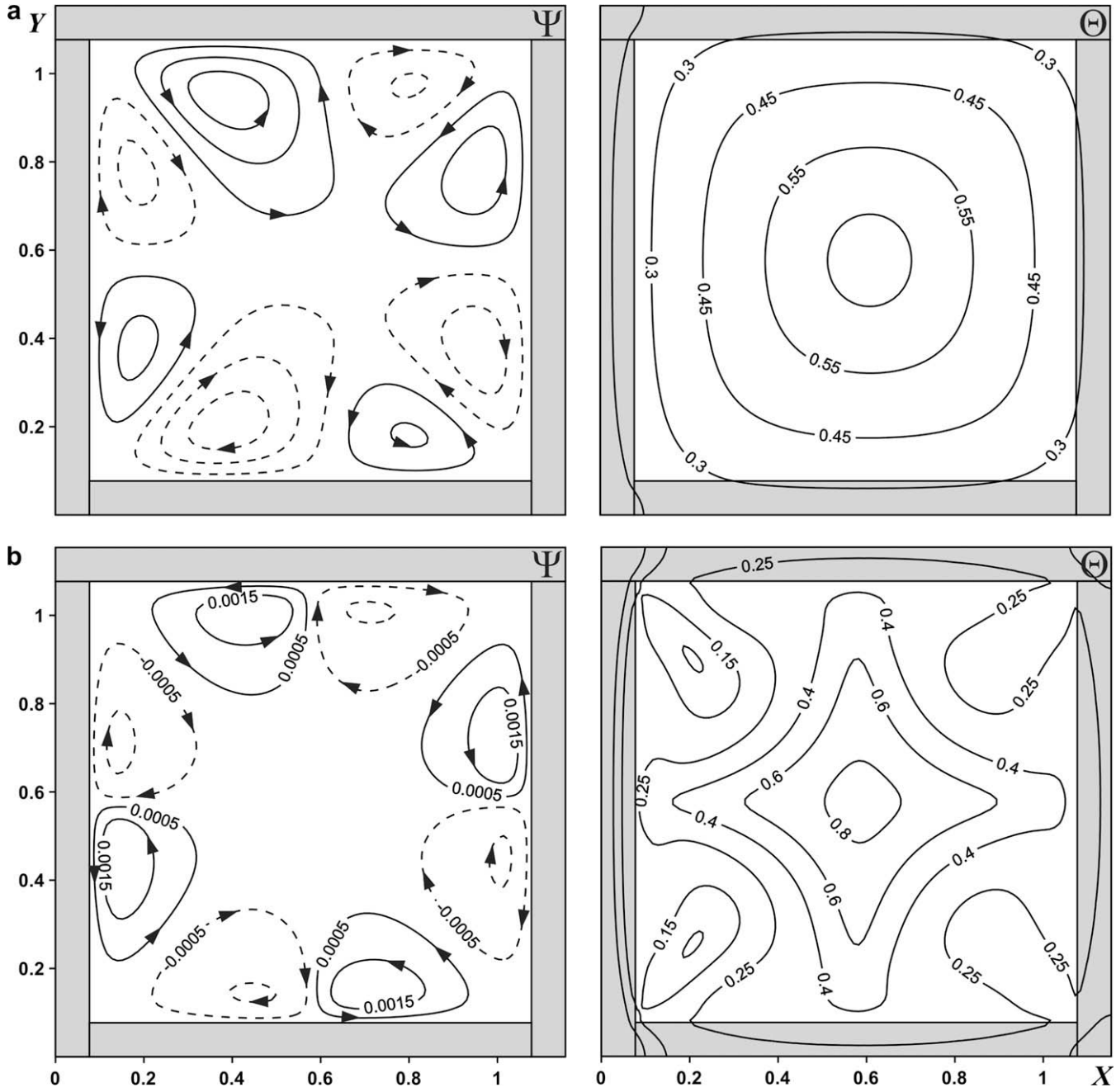

Fig. 3. Streamlines Ψ and isotherms Θ at $Z = 0.38$, $\tau = 300$, $\tau_\lambda = 50$, $k_{2,1} = 0.037$: $Gr = 10^5$ – *a*, $Gr = 10^7$ – *b*.

from the second circulation, has high flow velocities in the core and also covers a greater area. The reason for such asymmetry is penetration of the low temperature front from boundary $X = 0$ deep into the enclosure. The most intensive cooling of the gas cavity occurs in the zone of top left trihedral angle where the heat source influence is insignificant. At the same time interaction of high and low temperature areas reflecting in the displacement of "isotherms coordinate maximum" is visible. For example, "the coordinate top" of the isotherm corresponding dimensionless temperature ($\Theta = 0.1$) is displaced to the right wall.

The increase in the Grashof number up to $Gr = 10^7$ (Fig. 2, *b*) leads to essential modification of both streamlines and the temperature field. Two whirls are formed in the gas cavity. The whirls intensity has considerably increased. Spatial displacement and change of cores orientation of these convective cells are linked to the increased role of the buoyancy force. Position of the ascending and descending flows in the central part and on the peripheral zones of the gas cavity was conserved. Position of the ascending convective columns is caused by formation of the thermal plume above the heat source in its central part. There is more intensive heating of the top layer of the cavity owing to the increased velocities of the gas motion. For example, the isotherm corresponding dimensionless temperature ($\Theta = 0.3$) limits a greater area on the top of the cavity in comparison with the central cavity part. The latter is reflected in some deformation of the isotherm corresponding dimensionless temperature ($\Theta = -0.05$). This isotherm verges in the cavity to the solid wall surface. At the same time isotherms of the thermal plume near walls illustrate the presence of the descending convective flows.

Streamlines and temperature fields at $Z = 0.38$ are presented in Fig. 3.

The Grashof number ranging from 10^5 to 10^7 is reflected (Fig. 3) on the increase in the circulation velocities of the convective cells. The formation of the 8th-cellular steady hydrodynamic structure is observed. The temperature field is essentially changed. The thermal plume is formed in the centre of the gas cavity. There is the heating of the cavity from the thermal plume in a radial direction. Formation of original "thermal petals" in the zones of trihedral angles of the cavity is linked to the hydrodynamic structures of heat transfer process, namely with formation of the backward flows in these zones.

The temperature profiles at $Y = 0.3$, $Z = 0.38$, $\tau = 300$ and at different values of the Grashof number are shown in Fig. 4.

Fig. 4 shows the effect of the buoyancy force on the temperature field in the gas cavity. The increase in the Grashof number $10^5 \leqslant Gr \leqslant 10^6$ leads to monotonous increase in the temperature in the central part of the cavity where there is the thermal plume. The essential change of the temperature profile at $Gr = 10^7$ is linked to the increase in the gas motion velocities. Fall in the local temperature near the solid wall surfaces ($0.08 < X < 0.25$, $0.9 < X < 1.08$) at $Z = 0.38$ (Fig. 4, *a*) is caused by both the descending cold gas flows formation, and the energy redistribution along the vertical line of the gas cavity (Fig. 4, *b*). The high temperature at $0.3 < X < 0.8$ is explained by presence of the thermal plume in the centre of the cavity above the heater. Thus at $Z = 0.85$ essential

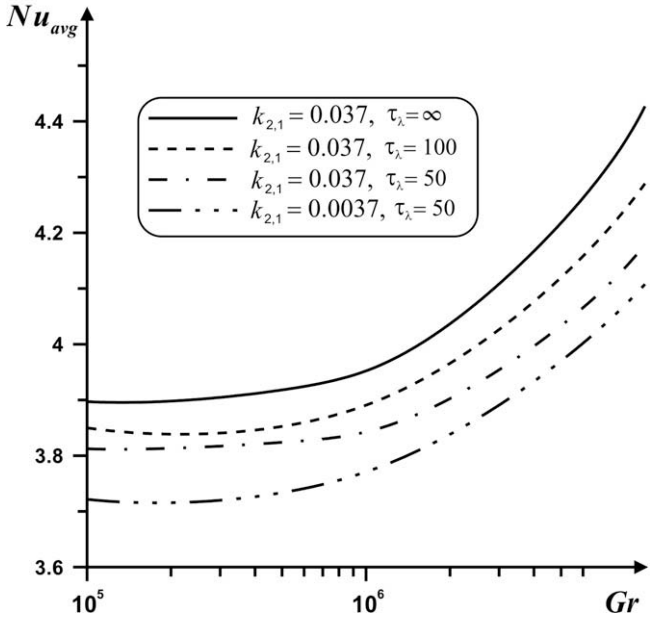

Fig. 5. Variation of the average Nusselt number versus the Grashof number, the optical thickness and the thermal conductivity ratio for $\tau = 300$.

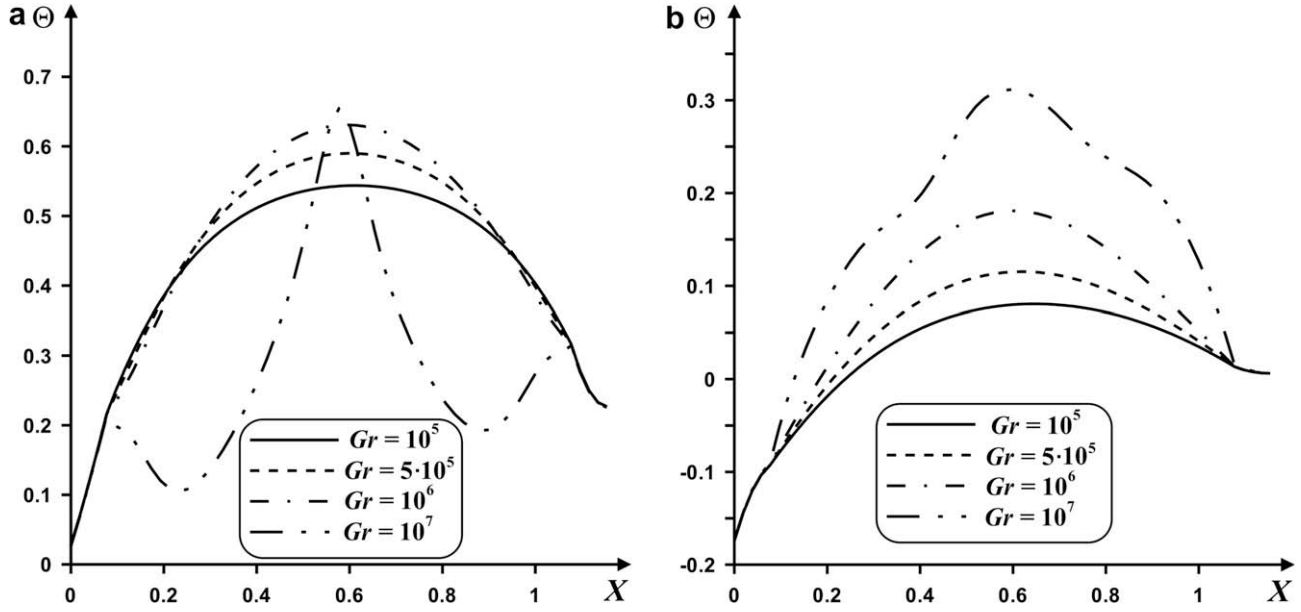

Fig. 4. Temperature profiles at $\tau = 300$, $\tau_\lambda = 50$, $k_{2,1} = 0.037$, $Y = 0.3$: $Z = 0.38$ – *a*, $Z = 0.85$ – *b*.

increase in the temperature at $Gr = 10^7$ is noticeable. The latter characterizes the increased value of the buoyancy force. The degree of the temperature pulldown (Fig. 4, *a*) at $Gr = 10^7$, $0.08 < X < 0.25$ is higher in comparison with the region $0.9 < X < 1.08$. This fact is caused by presence of the additional mechanism of the flow cooling at the solid wall $0 \leqslant X \leqslant 0.08$. The most intensive cooling of the wall $0 \leqslant X \leqslant 0.08$ is observed in the upper part of the solution region where influence of the heat source is sufficiently small (Fig. 4, *b*).

The analysis of the Grashof number influence on the generalized heat transfer coefficient (the average Nusselt number $Nu_{avg} = \int_{0.08}^{1.08}\int_{0.08}^{1.08} \left|\frac{\partial\Theta}{\partial Z}\right|_{Z=0.15} dXdY$) on the heat source surface has been carried out (Fig. 5).

The presented graphic dependences of the average Nusselt number as a function of the Grashof number evidently show the typical increase in the heat transfer intensity on the heat source surface at the Grashof number ranging $10^5 \leqslant Gr \leqslant 10^7$. The increase in a role of the buoyancy force in comparison with the internal friction force leads to the heat transfer intensification on the heater surface. The reason for this fact is both the increase in the motion velocities and more essential cooling of the descending gas flows. The latter leads to the significant heat sink from the heat source surface.

3.2. Effect of the transient factor

The transient factor in the conjugate heat transfer problems plays an essential role [20,22] as it reflects not only dynamics of the velocity and temperature fields in the gas cavity, caused by formation, evolution and dissipation of the vortex structures from

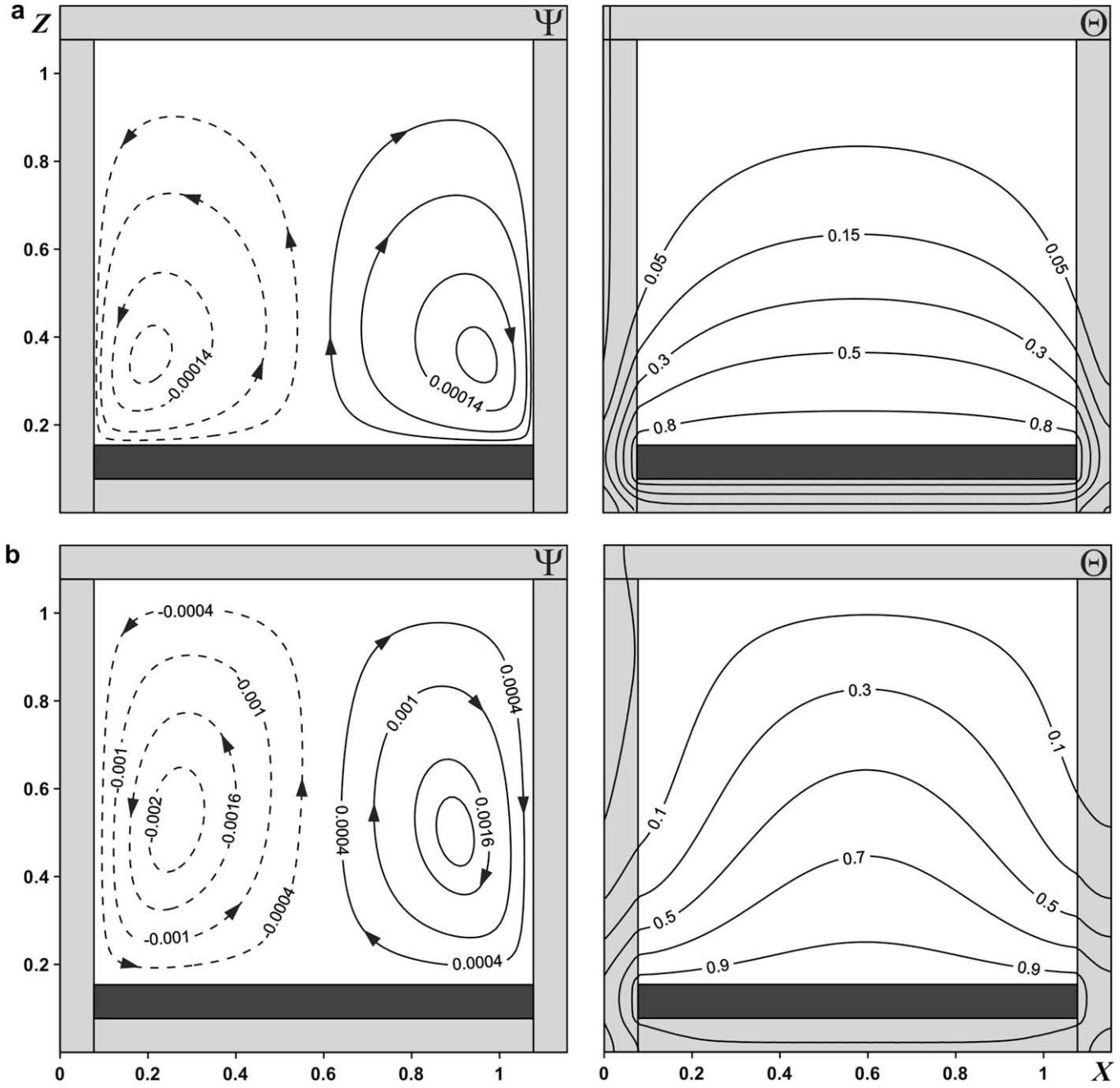

Fig. 6. The dynamics of streamlines Ψ and temperature fields Θ at $Y = 0.6$ for $Gr = 10^6$, $\tau_\lambda = 50$, $k_{2,1} = 0.037$: $\tau = 60$ – *a*, $\tau = 300$– *b*.

an initial quiescent state, but also it characterizes the thermal sluggishness of the solid walls in conditions of the environment influence. At the same time the advantage of such statement is definition of the temperature field at the solid–fluid interface on the basis of conservation laws without additional empirical data, for example, for the heat transfer coefficient. In turn the approach based on use of empirical heat transfer coefficients does not allow considering the transient factor as these coefficients are time functions.

The dynamics of the streamlines formation and temperature fields formation at $Y = 0.6$ for $Gr = 10^6$ are shown in Fig. 6.

There are two convective cells of small intensity in the gas cavity at $\tau = 60$ (Fig. 6, *a*). This fact is explained by the initial stage of the flow evolution. The temperature distribution is already non-uniformly. There is an intensive heating of the bottom of the cavity, but the thermal plume above the heat source hasn't yet formed. At the same time the cooling of the solid wall $0 \leqslant X \leqslant 0.08$ and, accordingly, the skew isotherms distribution in the left and right solid walls though thermal characteristics of these walls are identical is visible.

The increase in the time up to $\tau = 300$ leads to the increase in the velocities of the gas circulation. The cores of the convective cells are displaced in the geometrical middle of the areas surrounded by each whirl. The intensity of a motion in the left whirl is greater in comparison with another whirl. This fact can be explained as the low temperature front has reached the gas cavity in a zone of the left top angle. Formation of the thermal plume in the central part above the heat source is appreciable. The heating of the solid walls proceeds.

Evolution of the vortex structure and the temperature field at $Y = 0.3$ for $Gr = 10^7$ is presented in Fig. 7.

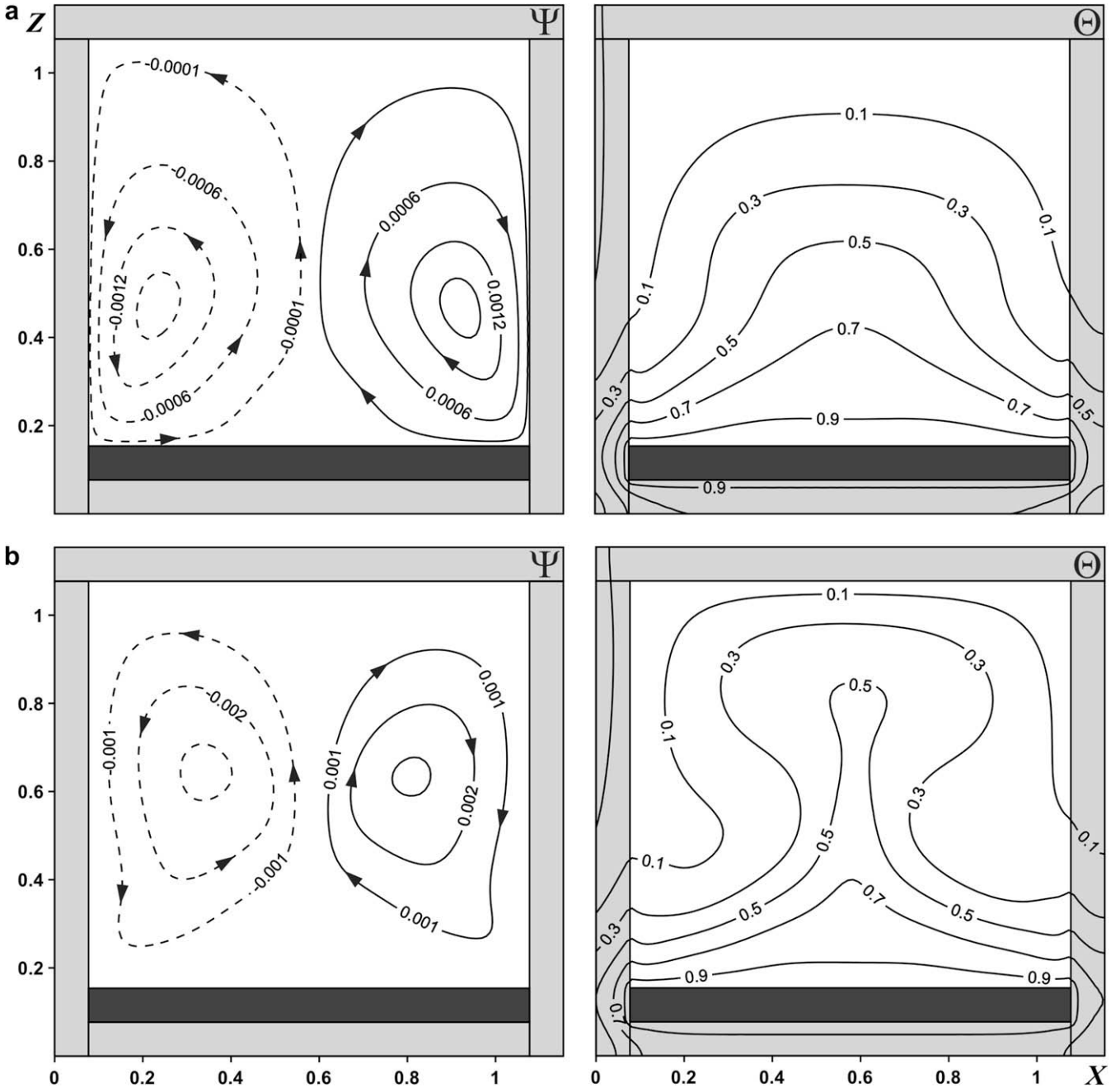

Fig. 7. The dynamics of streamlines Ψ and temperature fields Θ at $Y = 0.3$ for $Gr = 10^7$, $\tau_\lambda = 50$, $k_{2,1} = 0.037$: $\tau = 180$ – *a*, $\tau = 240$ – *b*.

The increase in the dimensionless time results both in displacement of the convective cells cores and in change of the hydrodynamic structures orientation different from Fig. 6. The dynamics of the temperature field differ from the mode for $Gr = 10^6$. The thermal plume, contributed the increase in the temperature in the cavity top layer, is formed at the heat transfer mode for $Gr = 10^7$ at $\tau = 240$.

The temperature profiles at $Y = Z = 0.6$ for $Gr = 10^7$ depending on time points are presented in Fig. 8. The increase in the dimensionless time leads to the increment in the temperature both in the gas cavity and in the solid wall $1.08 \leqslant X \leqslant 1.16$. There is fall in the temperature at $X = 0$ and, accordingly, cooling of the solid wall such as $0 \leqslant X \leqslant 0.08$ as the ambient temperature is below initial temperature of the solution region. Appearance of the local nonmonotonic zones at the solid walls surface at $\tau = 240$ is linked to an intensive motion of the descending flows.

The graphic dependences of the generalized heat transfer coefficient on the heat source surface versus dimensionless time and the Grashof number are presented in Fig. 9. The average Nusselt number Nu_{avg} decreases eventually at the fixed value of the heat conductivity ratio for $Gr = 10^5$, that is linked to heating the area near to the heater. Nonmonotonic change of Nu_{avg} for $Gr = 10^7$, possibly, is linked to the loss of stability of both the flow field and the temperature field, and as consequence, leads to formation of the transient laminar-turbulent mode.

3.3. Effect of the optical thickness

Taking radiation on the basis of Rosseland approach into account allows to estimate effect of this heat transfer mechanism due to a variation of the medium optical thickness $\tau_\lambda = \kappa_\lambda L_x$.

The convective heat transfer mode without radiation mechanism is a limiting case at $\tau_\lambda \to \infty$ if to judge by the equation (7). Thus, finite values of the optical thickness characterize presence of the monochromatic radiation. The increase in τ_λ from 50 to ∞ leads to the temperature pulldown in the gas cavity ($\max_{0 \leqslant X \leqslant 1.16} |\Theta_{\tau_\lambda = 50} - \Theta_{\tau_\lambda = \infty}| = 0.02, X = 0.6$, Fig. 10), and also it is reflected on increase in the generalized heat transfer coefficient at the heat source surface (Fig. 5).

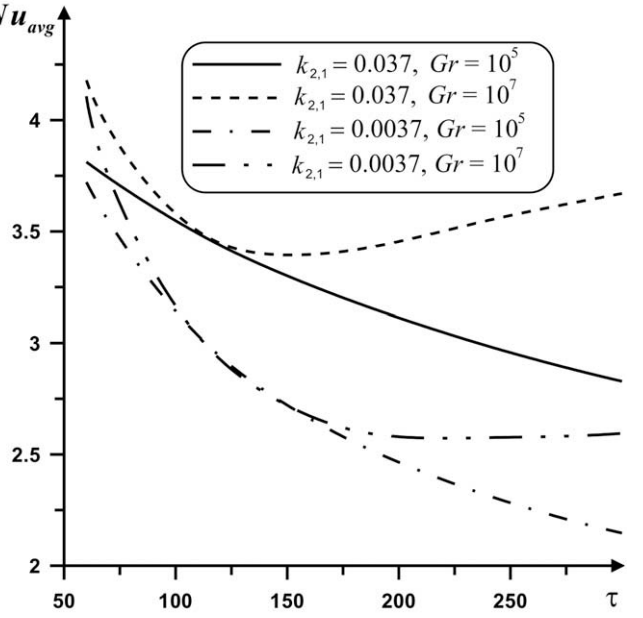

Fig. 9. Variation of the average Nusselt number with the dimensionless time at different values of the Grashof number and heat conductivity ratio.

3.4. Effect of the heat conductivity ratio

The thermal conductivity ratio characterizes the heat exchange conditions on the solid–fluid interface at analysis of the conjugate heat transfer. Accordingly, the variation of this parameter enables to define a range of change of the required characteristics.

The decrease in the thermal conductivity ratio (Fig. 11) leads to an intensification of the heat transfer in the solid walls, that is reflected on the increment in the temperature of the gas cavity. At the same time the average Nusselt number on the heat source surface decreases (Figs. 5 and 9).

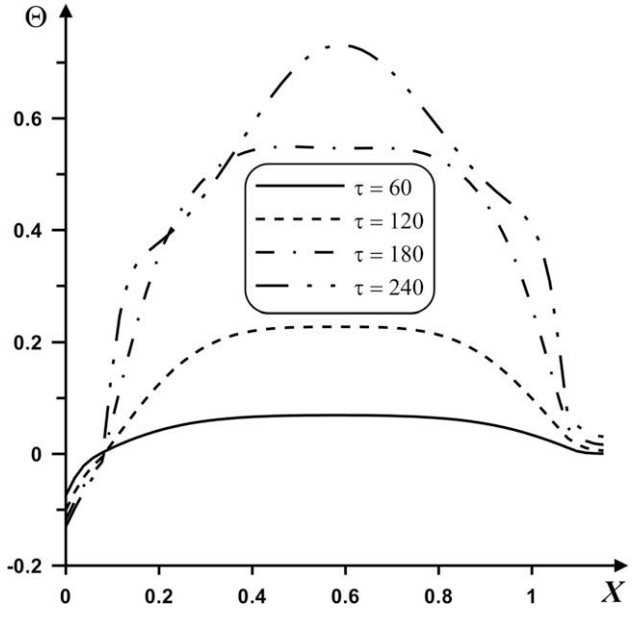

Fig. 8. The temperature profiles at $Y = Z = 0.6$ for $Gr = 10^7$, $\tau_\lambda = 50$, $k_{2,1} = 0.037$.

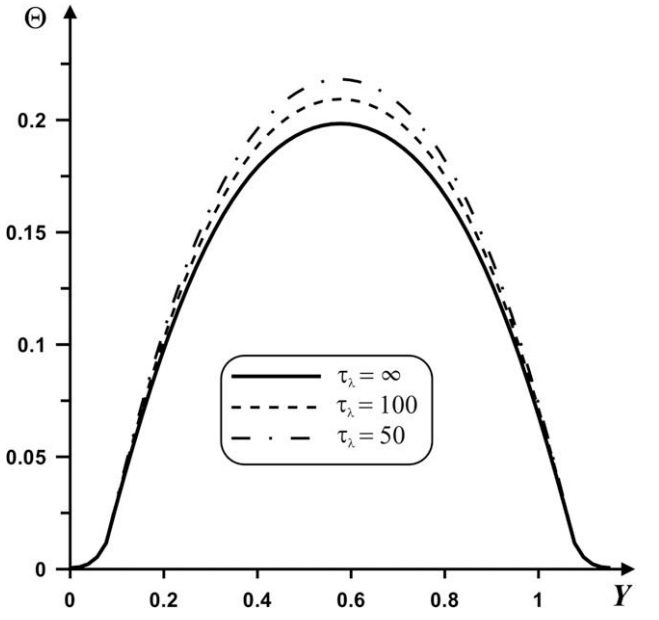

Fig. 10. The temperature profiles at $X = Z = 0.6$ for $Gr = 10^6$, $k_{2,1} = 0.037$ depending on the optical thickness.

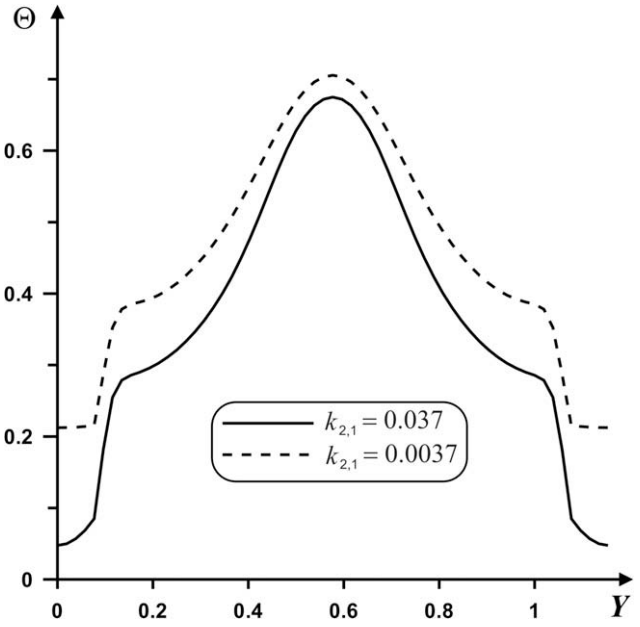

Fig. 11. The temperature profiles at $X = Z = 0.6$ for $Gr = 10^7$ *for,* $\tau_\lambda = 50$ depending on the heat conductivity ratio.

4. Conclusions

Mathematical simulation of the conjugate heat transfer in an enclosure having finite thickness walls in the presence of radiative heat transfer in a gas cavity has been carried out. The environmental effect has been considered in conditions of convective-radiative heat exchange on one of external boundaries of the solution region. Typical distributions of streamlines and temperature fields in wide enough range of defining parameters $10^5 \leqslant Gr \leqslant 10^7$, Pr = 0.7 have been obtained. The influence of the defining parameters such as the Grashof number, the transient factor, the optical thickness and the heat conductivity ratio on formation of thermo-hydrodynamic modes has been analysed. It is determined, that taking into account the radiative heat transfer leads to the temperature increase in the gas cavity at $0 < \tau < 200$ on the average on 11%. The further change of the dimensionless time leads to the temperature evenning (Fig. 10). The scopes of the nonlinear environmental effect, owing to conduction in the solid walls of the enclosure (Figs. 2, 3, 6 and 7) have been determined. It should be noted that the decrease in the heat conductivity ratio leads to reduction of the average Nusselt number on the heat source surface (Figs. 5 and 9).

Acknowledgement

This study has been supported by the Russian Foundation for Basic Research, through Grant No. 08-08-00402-a.

References

[1] S. Ostrach, Natural convection in enclosures, Adv. Heat Transfer 8 (1972) 161–227.
[2] A. Bejan, Convection Heat Transfer, Wiley, New York, 2004.
[3] K.T. Yang, Natural Convection in Enclosures Handbook of Single-phase Heat Transfer, Wiley, New York, 1987.
[4] Y. Jaluria, Natural Convection: Heat and mass transfer, Pergamon Press, 1980.
[5] B. Gebhart, Y. Jaluria, R.L. Mahajan, B. Sammakia, Buoyancy-induced Flows and Transport, Hemisphere Publishing, Corporation, 1988.
[6] O.G. Martynenko, P.P. Khramtsov, Free-convective Heat Transfer: With Many Photographs of Flows and Heat Exchange, Springer-Verlag, 2005.
[7] A.V. Luikov, Conjugate convective heat transfer problems, Int. J. Heat Mass Transfer 17 (1974) 257–265.
[8] A.V. Luikov, V.A. Aleksashenko, A.A. Aleksashenko, Analytical methods of solution of conjugated problems in convective heat transfer, Int. J. Heat Mass Transfer 14 (1971) 1047–1056.
[9] O. Aydin, Conjugate heat transfer analysis of double pane windows, Build. Environ. 41 (2006) 109–116.
[10] B. Premachandran, C. Balaji, Conjugate mixed convection with surface radiation from a horizontal channel with protruding heat sources, Int. J. Heat Mass Transfer 49 (2006) 3568–3582.
[11] A. Muftuoglu, E. Bilgen, Conjugate heat transfer in open cavities with a discrete heater at its optimized position, Int. J. Heat Mass Transfer 51 (2008) 779–788.
[12] D.M. Kim, R. Viskanta, Study of the effects of wall conductance on natural convection in differently oriented square cavities, J. Fluid Mech. 144 (1984) 153–176.
[13] A. Liaqat, A.C. Baytas, Conjugate natural convection in a square enclosure containing volumetric sources, Int. J. Heat Mass Transfer 44 (2001) 3273–3280.
[14] A. Liaqat, A.C. Baytas, Numerical comparison of conjugate and non-conjugate natural convection for internally heated semi-circular pools, Int. J. Heat Fluid Flow 22 (2001) 650–656.
[15] L. Valencia, J. Pallares, I. Cuesta, F.X. Grau, Turbulent Rayleigh–Benard convection of water in cubical cavities: a numerical and experimental study, Int. J. Heat Mass Transfer 50 (2007) 3203–3215.
[16] E.M. Sparrow, R.D. Cess, Radiation Heat Transfer, Brooks/Cole publishing company, Belmont, California, 1966.
[17] A.V. Luikov, Theory of Thermal Conductivity, Vysshaya shkola, Moscow, 1967.
[18] K. Aziz, J.D. Hellums, Numerical solution of the three-dimensional equations of motion for laminar natural convection, Phys. fluids 10 (1967) 314–324.
[19] P.H. Oosthuizen, J.T. Paul, Natural convection in a rectangular enclosure with two heated sections on the lower surface, Int. J. Heat Fluid Flow 26 (2005) 587–596.
[20] G.V. Kuznetsov, M.A. Sheremet, Conjugate natural convection in an enclosure with local heat sources, in: G. de Vahl Davis, E. Leonardi (Eds.), Proceedings of the Fourth International Symposium on Advances in Computational Heat Transfer, Begell House Publishers, 2008, p. 31.
[21] V.M. Paskonov, V.I. Polezhaev, L.A. Chudov, Numerical Simulation of Heat and Mass Exchange Processes, Moscow, Nauka, 1984.
[22] G.V. Kuznetsov, M.A. Sheremet, Modelling of thermogravitation convection in closed volume with local sources of heat release, Thermophys. Aeromech. 13 (2006) 565–574.
[23] O.A. Bessonov, V.A. Brailovskay, S.A. Nikitin, V.I. Polezhaev, Three-dimensional natural convection in a cubical enclosure: a benchmark numerical solution, in: G. de Vahl Davis, E. Leonardi (Eds.), Proceedings of the First International Symposium on Advances in Computational Heat Transfer, Begell House Publishers, 1997, pp. 157–165.
[24] T. Fusegi, J.M. Hyin, K. Kuwahara, A numerical study of 3D natural convection in a differently heated cubical enclosure, Int. J. Heat Mass Transfer 34 (1991) 1543–1557.
[25] W.H. Leong, K.G.T. Hollands, A.P. Brunger, Experimental Nusselt numbers for a cubical-cavity benchmark problem in natural convection, Int. J. Heat and Mass Transfer 42 (1999) 1979–1989.
[26] D.A. Kaminski, C. Prakash, Conjugate natural convection in a square enclosure effect of conduction on one of the vertical walls, Int. J. Heat Mass Transfer 29 (1986) 1979–1988.